Comprehensive Experimental Investigation of Flow Boiling Performance in a Single Microchannel Utilizing Silver and Multi-Walled Carbon Nanotube Hybrid Nanofluids

Shahid Mahdy Talib [1,2*] , Ekhlas M Fayyadh[2] , Moayed R Hasan[2]
[1,] Ministry of education, general directorate for vocational education, Karbala 56001, Iraq
[2] Mechanical Engineering Dept, University of Technology-Iraq, Baghdad 10066, Iraq
Corresponding Author Email: me.20.18@grad.uotechnology.edu.iq

Abstract
This study investigates the occurrence of flow boiling in a microchannel with a uniform cross-sectional area. The primary emphasis is placed on the attributes and qualities of deionized water when it is subjected to temperatures lower than its boiling point. The experiments utilized deionized water as the working fluid in a rectangular microchannel with a consistent cross-sectional shape. The experiments were conducted at an input temperature of 80°C, with a mass flux of 200 kg/m²s and a heat flux ranging from 1.735 to 625.1 kW/m². The increase in wall superheat is exactly proportional to the increase in heat flow, indicating that the onset of nucleate boiling (ONB) occurs at a far lower point in nanofluid channels compared to bare channels. The observed rise in heat transfer coefficient (HTC) at a mass flow rate of 200 kg/m²s suggests that nanofluids in microchannels demonstrate a similar pattern to microchannels without nanoparticles. The average heat transfer coefficient (HTC) for microchannels filled with nanofluids containing silver (Ag), multi-walled carbon nanotubes (MWCNTS), and a combination of Ag and MWCNTS (in a 1:1 ratio) is enhanced by 9%, 14.5%, and 18.01%, respectively, compared to the microchannel without any additives.
The pressure drop decreases significantly as the wall heat flux increases due to the reduced viscosity of the liquid. However, the phenomenon of pressure decrease experiences a change throughout the boiling process. The pressure reduction in microchannels containing nanofluids has a similar trend to that of the microchannel without any additives, where an increase in heat flow corresponds to an increase in pressure drop. The pressure drop for Ag, MWCNTS, and the Ag plus MWCNTS mixture is respectively 3.3%, 4.4%, and 10.4% higher compared to the bare channel. This study provides valuable insights into the behavior of deionized water and nanofluids in microchannels under various heat conditions.

Keywords:-single microchannel, flow boiling, hybrid nanofluid, heat transfer coefficient

1. Introduction

Microchannel heat exchangers (MHEs) have an extremely high surface-to-volume ratio, which makes it possible for them to move heat much faster than regular heat exchangers. Therefore, in microchannels, using a single-phase flow can result in heat dissipation of approximately 10 MW/m^2, as stated by Kandlikar (2003) [1]. An uneven distribution of temperatures and a severe pressure drop unfortunately accompany this. Based on that, investigation over the past two decades has concentrated on investigating flow boiling in MHEs as a means of cooling systems with increased heat flux, including insulated laser diodes, fuel cells, gate bipolar transistors (IGBTs), and electronic devices. Additionally, flow-boiling's primary advantages in these devices are summed up below: (1) Flow boiling can cause a modest alteration in the surface temperature. The longevity of electronic devices is greatly improved by reducing thermo-mechanical stresses in the chip. (2) In order to achieve a highly compact and cost-effective cooling system, a small pump for liquid pumping is required. Even though flow boiling in microchannel heat sinks (MHSs) has clear benefits, some critical problems remain unaddressed. A few examples of these issues are as follows: (1) Early dry-out due to low critical heat flux; (2) Start-up boiling is the requirement for a significant increase in wall temperature, known as wall superheat, to reach the point where boiling begins. (3) Flow reversals and instabilities. (4) The boiling properties of microchannel flow are

ambiguous. Many flow-boiling studies in conventional microchannels reveal that at low heat flows, mass flux has no impact. In contrast, increases in mass flux caused important improvements in the coefficient of heat transfer at fluxes with high heat or when the main type of flow seen in the channels was convective boiling. In their 2008 study, Harirchian and Garimella [2] conducted tests at various mass fluxes with FC-77. They determined that the heat transfer coefficient was maintained after nucleate boiling started, no matter what the mass flux was. Besides this, when the heat fluxes reached the point where bubble formation was prevented at the channel walls (as viewed in the flow visualization), greater coefficients of heat transfer were achieved under conditions of higher mass flux. In a silicon MHS under sub-cooled conditions, Huang et al. (2016) looked into the properties of the boiling flow of R1233zd(E) using various mass flux ranges. According to their report, in the region with very low vapor quality and a subcooled area, keeping heat flux constant, local heat transfer declined slightly. The mass flux rose. However, the coefficient of local heat transfer showed a substantial increase with rising mass flux in the region with vapor of relatively high quality. In a heat sink with microchannels operating with distilled water as its fluid, the coefficients of heat transfer in two-phase significantly rise with a higher mass flux. This has been seen in studies conducted by Markal et al. (2016) [4], Mohammed and Fayyadh (2020) [5], and Al-Nakeeb et al. (2023) [6]. Some studies, including Al-Zaidi et al., 2019 [7], have found a weak relationship between the mass flux and the coefficient of heat transfer when utilizing straight microchannel heat sinks. With mass fluxes ranging from (50 kg/m^2.s) to (250 kg/m^2.s) and wall heat fluxes ranging from (25.1 kW/m^2) to (191.6 kW/m^2), respectively, and under subcooled conditions, they studied, in a heat sink with a multi-microchannel, the HFE-7100 flow boiling heat transfer. Contrarily, research by Harirchian and Garimella (2008) [8] and Bertsch et al. (2009) [9] observed that, in most cases, the two-phase value was unaffected by mass flux. Whereas, in the low heat flux zone, they found slightly greater coefficients of heat transfer as mass fluxes decreased. The mass flux impact on the quality of vapor at the channels' exits was thought to be responsible for this. Also, using R134a as the operating fluid, Fayyadh et al. 2017 [10] did studies in a multi-microchannel for a mass flux and range of heat flux. Mass flux affects the quality of channel vapor. In flow-boiling systems, heat transfer's main procedure requires evaluating how the heat transfer factors change over time with mass flux.

An additional mass flux consequence is that faster rates of heat transfer in the microchannels will worsen while the mass flux rises. Coefficients of heat transfer between 594 kg/m^2.s and 1051 kg/m^2.s declined with increasing mass flux at low vapor quality, according to Costa-Patry et al., 2011 [11], owing to more intermittent dry-out and early bubble coalescence.

The range of heat flux into the channel may also affect the mass flux effectiveness. **Agostini et al. (Part I), 2008 [12]** showed that the mass flux effect was merely visible for (R245fa) when the flux of heat fluctuated between medium and high and when the heat flux was high for (R236fa). This might be because of the variations in fluid properties that create fluctuations in the dynamics of the extended bubbly flow. For a particular heat flux, Alam et al. (2016) [13] found that raising the mass flux up to 400 kg/m^2.s increased the average coefficients of transfer of heat in the array of silicon nanowire microchannels to their maximum, while further increasing the mass flux caused a major decline.

Based on previous research, it has been demonstrated that utilizing microchannels significantly enhances heat transfer due to their high surface-to-volume ratio, enabling more efficient cooling in systems with high heat flux. Additionally, nanofluids have proven to be an effective method for augmenting heat transfer in conventional thermal systems. However, combining microchannel technology with hybrid nanofluids is expected to result in a synergistic improvement in thermal performance. Hybrid nanofluids possess superior thermal properties compared to the individual nanofluids from which they are derived.

In this study, hybrid nanofluids composed of silver (Ag) and multi-walled carbon nanotubes (MWCNTs) were selected to evaluate their performance within a single microchannel under two-phase flow conditions. The aim is to assess the capability of these hybrid nanofluids to enhance heat transfer and reduce pressure drop, compared to microchannels utilizing conventional fluids or single-component nanofluids. This research will provide a deeper understanding of the thermal

mechanisms at play in micro-scale systems and offer insights into optimizing cooling efficiency for high heat flux applications involving two-phase flow.

2. Experimental Facilities

Various mass fluxes have been experimentally studied to see how they affect the boiling flow feature in a single microchannel. A wide range of tools and resources were needed to finish it. The lab of the University of Technology's Mechanical Engineering Department was the site of the experimental investigation.

Figure (1) and Plate (1) show the experimental facility, which includes the electrical power supply, auxiliary cooling loop, testing flow loop, degase unit, and measuring equipment. A main tank, electrical preheater, micro-gear pump, test section, filter, and sub-cooler were the primary components of the closed-loop testing loop. A closed-loop auxiliary cooling system was depicted by the chiller unit.

This work also included the design and manufacturing of the test section which shown in the Figure (2). The components include a housing, an O-ring, thermocouples, a mica layer, a cartridge heater, and a brass block.

A 30 mm wide, 114 mm long, and 81 mm high copper block with two subchannels (one connected to the microchannel's outlet and the other to its inlet), a single rectangular microchannel on top, and the manifold's outlet and inlet connected to the subchannels' inlets and outlets. The nominal microchannel width is 0.7 mm, and the nominal microchannel depth is 0.3 mm. Both the inlet and the outlet subchannels, whose width and length are 2 mm and 7 mm, respectively, are of the same depth as the microchannel. The inlet and outlet manifolds' dimensions are 10 mm in depth, 20 mm in width, and10 mm in length. Using a 10 mm/min feeding rate and a cutting machine, a single rectangular microchannel was cut off, a subchannel on each side of it, and the manifold from the top face of the brass block. The brass block was heated by drilling two 8-mm-diameter holes near the base of the block, into which were inserted two cartridge heaters oriented horizontally and parallel to the microchannel. The heating capacity of each cartridge heater is 100 W. A total of four type K thermocouples were evenly spaced 14.7 mm apart and inserted vertically along the middle of the brass block. This measurement was taken to determine the heat flux. Seven thermocouples of type K were put evenly along the length of the microchannel and spaced 1 mm below it. The distance between each thermocouple was 9.67 mm. Along the microchannel's axial direction, the determination of the coefficient of transfer of local heat was their purpose. Two thermocouples of type K were utilized for the measurement of the temperature of working fluid at the test section's outlet and inlet. At the inlet manifold, one was inserted into an opening that is 1 mm in diameter, and at the outlet manifold, the other was inserted. One-half millimeter is the diameter of each thermocouple utilized within the brass block. Each inlet/outlet manifold location had a hole drilled with a diameter of 3 mm to find out how much pressure dropped in the test area. To further fix the leakage that occurs between the housing and the upper cover of the microchannels, on top of the brass block, an O-ring slot was cut out..

The heated brass block was encased in mica layers on all sides to stop heat loss to the immediate vicinity. The assembly was subsequently installed into the housing component. Crafted from stainless steel (SS), it was specifically tailored to fit the test section within the testing loop. The housing underwent drilling of 1 mm and 5 mm in diameter, respectively, to accommodate the thermocouple and pressure device wires. A stainless-steel top cover and screws were then used to seal the assembly.

3. Nanofluid preparation

Acquired nanofluid formulations from VCN Materials. The properties of Dione's water at 25°C are the following: viscosity of 0.89 cP, density of 998 kg/m3, specific heat of 4200 J/kg.K, and thermal conductivity of 0.607 W/m.K. This experiment employs a two-step method for preparing nanofluids.

In order to create nanofluids, the required amount of nanoparticles was measured using a weight device and then dispersed in deionized water, which was quantified using an analytical balance made by Precisa in Switzerland. Subsequently, the samples were agitated for a duration of 60 minutes using a magnetic stirrer. A homogeneous and stable nanofluid was generated using the ultrasonication probe (QSonica, USA; Hielscher UP400S, 400 W, 24 kHz, Germany). Stirring with a stirrer for 60

minutes at a speed of 1200 revolutions per minute. The nanofluids that were agitated underwent ultrasonication for a duration of 2 hours using a 700 W, 20 kHz digital sonicator. This process was carried out to disintegrate large particle agglomerations and produce a sample that remained free of silt for a prolonged period of time. A 550-watt ultrasonic probe was used for a duration of 60 minutes to achieve stability in nanofluids. There was no 24-hour period of settling. The stability test consisted of acquiring a minute sample of nanofluid and visually inspecting it for any signs of sedimentation. There was an absence of sediment. The materials were fabricated in dedicated nanotechnology laboratories.

4. Reduction of Data

4.1 The single-phase flow

Across the microchannel, the decrease in pressure, as shown by ΔP_{ch}, is determined by:

$$\Delta P_{ch} = \Delta P_{m}\text{-} \qquad \Delta P_{loss} \quad (1)$$

Where ΔP_{m}- refers to the change in pressure across the test segment. ΔP_{loss} refers to the decrease in pressure because of small losses. It is determined using the formula given below:

$$\Delta P_{loss} = \Delta P_{sch,i} + \Delta P_{sch,o} + \Delta P_{sc} + \Delta P_{se} \quad (2)$$

Where $P_{sch,o}$ and $\Delta P_{sch,i}$ refer to the subchannel's pressure drop at its outlet and its inlet, respectively. While ΔP_{sc} and ΔP_{se} refer to pressures caused by the sudden shortening and the sudden widening, respectively.

At a minimum Re of 166.5 and a maximum Re of 2393, the losses because of the subchannel's outlet and inlet were 2.3% and 0.26%, respectively; because of this, they went unnoticed. Hence, the following is the drop in pressure caused by every minor loss from abrupt expansion and contraction, as calculated using the equation below:

$$\Delta P_{loss} = (\mathrm{K}sc_2 + \mathrm{K}se_1)\frac{f}{2} * V^2 ch_{\square} + (\mathrm{K}sc_1 + \mathrm{K}se_2)\frac{f}{2} * V^2 sch_{\square} \quad (3)$$

The coefficients of loss because of the sudden contraction at the test section's inlet, which passes through the manifold, subchannel, and microchannel, are represented by (Ksc1 & Ksc2). Alternatively, the coefficients of loss due to the sudden expansion are shown by (Kse1 & Kse2). It starts at the outlet of the microchannel and moves to the subchannel and, finally, the manifold. Additionally, the coefficients of loss are 0.5 for Ksc1, 0.47 for Ksc2, 0.72 for Kse1, and 0.81 for Kse2., as stated in [5]. ($\grave{q}_b$)

On the base heat sink, the heat flux can be found by the following formula:

$$\grave{q}_b = \frac{(P - Q_{loss})}{A_b} \quad (4)$$

$$P = I .V \quad (5)$$

Where V, I, and P denote the voltages (volts), electric current (ampere), and heating power (watts), respectively. According to the equation below, the heat sink's base area is denoted as, A_b:

$$A_b = W_b * L_b \quad (6)$$

Where, L_b and W_b are the base heated block's length and width, respectively.

The heat losses (Q_{loss}) from the section of the test to the immediate vicinity were measured by heating the test section without any flow using the turn-off gear pump. The microchannel's heating power and temperatures were then recorded when the system reached a steady state. By doing this process over and over, different amounts of electricity were also tested. The heat loss formula was then derived by comparing the ambient and brass block temperatures with the applied electrical power. This method was detailed by researchers in their publications [5] and [6].

The (h_{sp}(z)) coefficient of local heat transfer is determined as:

$$h_{sp}(z)) = \frac{\grave{q}_b * W_b}{\left(T_W(z) - T_f(z)\right) * (2 * H_{ch} + W_{ch})_{\square}} \quad (7)$$

A conduction equation of one dimension was applied to change the microchannel's temperature of a local wall ($T_W(z)$) at an axial location (z), as determined using the following formula:

$$T_W(z) = T_{tc}(z) - \frac{\grave{q}_b * th}{K_{br}} \quad (8)$$

Where, $T_{tc}(z)$ refers to the thermocouple's local temperature positioned at a (th) distance, corresponding to 1 mm below the microchannel. Furthermore, by applying an energy balance and presuming boundary conditions of homogeneous heat flux, the fluid's local temperature ($T_f(z)$) may be determined using equation (9):

$$T_f(z) = T_i + \frac{\grave{q_b}*(W_b .z)}{\dot{m}C_P} \quad (9)$$

The average Nusselt number was determined utilizing the equation that follows:

$$N_u = \frac{1}{L_{ch}} \int_0^{L_{ch}} \frac{h_{sp}. D_h .dz}{K_f} \quad (10)$$

4.2 The two-phase flow

Subcooled fluid is the working fluid state condition at the inlet microchannel. At the microchannel inlet, the working fluid is a one-phase case until thermodynamic equilibrium is achieved (0). After this, the boiling phenomenon begins. Hence, two zones can be defined by the microchannel's length: The single-phase zone has a length of L_{sp}, whereas the two-phase zone has a length of (L_{ch}-L_{sp}). The thermodynamic quality position, represented by the value of 0, indicates the exact point of division between two distinct zones. Furthermore, the below formulae can be utilized to compute the drop in pressure in different regions and the coefficient of heat transfer:

The drop in pressure at a single phase can be calculated by:

$$\Delta P_{sp} = \frac{2 f_{app} G^2}{\rho_l D_h} L_{sp} \quad (11)$$

This formula was utilized to determine the apparent friction factor f_{app} using the developing flow equation given by [5]:

$$f_{app} = \frac{3.44}{Re(L^*)^{1/2}} + \frac{(f_{FD}Re) + \frac{K(\infty)}{4L^*} - \frac{3.44}{(L^*)^{1/2}}}{Re(1 + C(L^*)^{-0.2})} \quad (12)$$

$$L^* = L_{sp}/ReD_h \quad (13)$$

The constants ((C) and K (∞)) rely on an aspect ratio. The amounts are (1.1972) and (1.7784 x 10-4) for the geometry used in this study, respectively [6]. Furthermore, the Poiseuille number (f_{FD}Re) was provided via **[5]** regarding the fully evolved single-phase fluid flow**:**

$$(f_{FD}Re) = 24(1 - 1.35534\beta + 1.9467\beta^2 - 1.7012\beta^3 + 0.9653\beta^4 - 0.2537\beta^5) \quad (14)$$

The aspect ratio for the microchannel, denoted by (β) in the overhead formula, was calculated using:

$$\beta = \frac{w_{ch}}{H_{ch}} \quad (15)$$

Also, this formula was utilized to determine the single-phase length (L_{sp}):

$$L_{sp} = \frac{\dot{m}C_p(T_{sat} - T_i)}{q_b^{"} W_b} \quad (16)$$

Then, the drop in pressure of the two-phase region (ΔP_{tp}) in the microchannel is given by:

$$\Delta P_{tp} = \Delta P_{ch} - \Delta P_{sp} \quad (17)$$

The coefficient of transfer of heat in the two-phase zone is expressed as:

$$h_{tp}(z) = \frac{q_b^{"} W_b}{(T_w(z) - T_{sat}(z))(W_{ch} + 2H_{ch})} \quad (18)$$

The fluid's local saturation temperature is denoted by, $T_{sat(z)}$. According to reports in [5] and [6], it was calculated utilizing the local pressure, which was acquired using the assumption that the pressure drops linearly along the microchannel's length.

$$P_{tp}(z) = P_{sat}(L_{sp}) - \left(\frac{z - L_{sp}}{L_{ch} - L_{sp}}\right) \Delta P_{tp} \quad (19)$$

Additionally, this formula was used to calculate the vapor's thermodynamic quality at each axial location x(z):

$$x(z) = \frac{i(z) - i_l(z)}{i_{ig}(z)} \quad (20)$$

Where ($i_{ig}(z)$ and $i_l(z)$) denote the vaporization latent heat y and the liquid-specific enthalpy,

respectively, which are computed using the formula (19) at microchannel local pressure. At the location (z) adjacent to the microchannel, the enthalpy of the fluid, denoted as $i(z)$, was determined using the energy balance in this equation:

$$i(z) = i_i + \frac{q_b^{"} W_b}{\dot{m}} \quad (21)$$

The symbol i_i represents the inlet's specific enthalpy, which can be foung by gauging the pressure and temperature at the test section's inlet.

4.3 Uncertainty Analysis

The difference between the measured and actual quantities of a quantity is known as the measurement error. Several factors can contribute to this, such as systematic bias and chance error. Calibration of devices helps reduce bias errors, which are caused by measurement inaccuracies. Errors in accuracy (random) can be caused by environmental variables such as humidity, temperature, and pressure. Assessed utilizing the technique introduced via [6].

5. Result and Discussion

5.1 Single-Phase Flow and Heat Transfer

Earlier than initiating the tests of two-phase flow boiling, experiments were conducted to study single-phase flow. These tests were performed at various Reynolds numbers, with 1 bar of pressure in the system, under both diabatic and adiabatic circumstances. The purpose of this was to guarantee that the instruments work as intended and provide accurate results. The experiments were conducted in a standard microchannel with a Reynolds number range of 166.5 to 2547 and an intake temperature of 30 °C, determined by the hydraulic diameter. To estimate the friction factor and Nusselt number, the experimental data stood in comparison to previous work that used a plain microchannel and found correlations. For both conventional and microchannels, these relationships were postulated. Additionally, the comparisons were assessed by the mean absolute error (MAE) of Fayyadh. et al. 2017 [10] in the following way:

$$MAE = \frac{1}{N}\sum_{j=1}^{N} \frac{|\theta_{pred,j} - \theta_{exp,j}|}{\theta_{exp,j}} \; x100\% \quad (22)$$

Wherein:

Θ: indicates either the Nusselt number or the Fanning friction factor.

N: data point quantity.

For the four models, Figure (3) depicts the Reynolds number versus the experimental Fanning friction factor. The correlation of Shah and London (1978) [14] provided a satisfactory correlation with a mean absolute error (MAE) of 1.89% at the same period with respect to laminar developing flow. Additionally, they discovered that the data supported the correlation. Conversely, Blasius (1913) [15] predicted the experimental results for two models at a turbulent zone in fully matured using correlations, and the mean absolute error (MAE) was approximately 2.57%. The correlation analysis carried out by Phillips (1987) [16] demonstrated precise estimation with a mean absolute error (MAE) of 2% during the time when there was a turbulent developing flow. The relationship between the study outcome and the prior experimental data of Q. A. Al-Nakeeb [17] is deemed satisfactory, with a mean absolute error (MAE) of 8.07%, which is higher than that of H. Q. Hussein[18],] with a mean absolute error (MAE) of 2.9%.

The experimental average Reynolds number versus the Nusselt number can be shown in Figure (4). The present study's findings, in contrast to the data anticipated by Shah and London correlations [14] for completely developed flow, reveal an inadequate estimate with a mean absolute error (MAE) of 26.13%. While comparing the results of the simple microchannel with the correlations presented by Shah and London [14] for developing flow, an MAE of 15.12% was predicted. In the meantime, Mirmanto's [19] assessment of microchannel correlations revealed a low MAE of 25.63% and 59.54% for the outcomes of plain microchannel predictions. This may be attributed to the fact that the connection disregarded material influence.

The figure clearly shows that the current work's results were satisfactory in comparison to prior experimental data by H. Q. Hussein [18], with a mean absolute error (MAE) of 4.46%. Finally, it is clear from the single-phase flow investigations that the system of measurement and calibration can deliver satisfactory findings for the experiments with two-phase flow.

5.2Two-Phase Results

The present work involves an experimental exploration of the transfer of boiling heat, subcooling flow, and drop in pressure of deionized water in a single microchannel across a mass flux of 200 kg/m^{2}s. Heat flux varied from 1.7 kW/m^2 to 650 kW/m^2. The inlet temperature was set to 80°C, while keeping the inlet pressure at 101.325 kPa.

The influence of nanofluids in microchannels on the boiling curve is exhibited in **Figure (5).** At identical operating conditions (mass flux of 200 kg/m^{2}s and degree of subcooling of 20 K), **Figure (5)** examines the curves of boiling for the bare microchannel and nanofluids at the dimensionless site of Z/L = 0.98, which is close to the microchannel's exit. Based on the figure, the boiling curve of nanofluids followed a pattern equivalent to a bare channel, with a little leftward shift. Researchers like Benkheira et al. (2006) [20] discovered this finding. There is a considerable reduction in the ONB for nanofluid channels as compared to bare channels. For example, the wall superheat is approximately 1.8, 1.65, 1.3, and 0.77 K for the bare and **Ag**, MWCNTS and **Ag** WITH MWCNTS (1:1) nanofluids microchannels, respectively. The result is that the wall superheat was reduced due to the presence of nanofluids in the microchannel. Hence, the percentage reduction in wall superheat for coated channels by **Ag**, MWCNTS and **Ag** WITH MWCNTS (1:1), respective to the plain channel, was 10.8%, 20.2%, 58.3%, respectively. . Same as in **Balasubramanian et al. (2013) [21] and Qu and Mudawer (2003) [22].**

The change in HTC with the heat flow for bare and **Ag**, MWCNTS and **Ag** WITH MWCNTS (1:1) appears in Figure (6). At a dimensionless site (Z/Lch = 0.98, which is close to the microchannel's exit), the findings were given for a degree of subcooling of 20K and a mass flux of 200 kg/m^{2}s. Compared to the bare microchannel, the HTC for the nanofluid microchannel follows a comparable pattern, as can be seen in the figure. Unlike the bare microchannel, the average HTC for three nanofluid microchannel models with **Ag**, MWCNTS and **Ag** WITH MWCNTS (1:1)is enhanced by 9%, 14.5%, and 18.01%, respectively, including **Qu and Mudawar (2004) [22] and Harirchian and Garimella (2008) [23].**

Figure 7 indicates the association between the drop in pressure and the heat flux for the baree channel and the nanofluid channel. With a subcooling degree of 20 K and a mass flux of 200 kg/m^{2}s, the outcomes were given. The drop in pressure for the nanofluid microchannel follows a pattern comparable to that of the bare microchannel, as shown in the figure. Three models showed a rise in the drop in pressure as the heat flux rose. For instance, the drop in pressure for nanofluid **Ag**, MWCNTS and **Ag** WITH MWCNTS (1:1) relative to the bare channel is 3.3%, 4.4%, and 10.4%, respectively. Researchers such as Harirchian and Garimella (2008) [23] and Mohammed (2020)[24] discovered this observation.

6. Conclusions

The present investigation analyzed the occurrence of flow boiling in a single microchannel with a consistent cross-sectional area, specifically concentrating on the characteristics of deionized water at sub-cooled temperatures.
The experiments were conducted using deionized water as the working fluid in a single rectangular microchannel with a uniform cross-sectional area. The experiments were conducted at an inlet temperature of 80°C, with a mass flux ranging from 200 kg/m2·s and a heat flux ranging from 1.735 kW/m2 to 625.1 kW/m2.
The findings of the current investigation are given, resulting in the following conclusions:
1. It is evident that the wall superheat rises proportionally with the increase in heat flux. Furthermore, it is evident that the ONB for nanofluids channel experiences a substantial decrease in comparison to a bare channel.
2. The heat transfer coefficient is increased when the mass flow rate is 200 kg/m2s. The trend of the heat transfer coefficient (HTC) for nanofluids in a microchannel is evidently identical to that of the bare microchannel. The average heat transfer coefficient (HTC) is increased by 9%, 14.5%, and 18.01% in three nanofluid microchannel models containing Ag, MWCNTS, and Ag with MWCNTS (1:1), respectively, compared to the bare microchannel. There is a substantial reduction in pressure drop as the heat flux on the wall is increased. This is due to a decrease in the viscosity of the liquid. Subsequently, the pressure drop pattern will change once boiling occurs. The pressure drop in a microchannel for nanofluids has a comparable pattern to that of the bare microchannel. The

pressure drop exhibited an increase in three models as the heat flux was increased. The pressure drop for nanofluids in a microchannel is as follows: for Ag nanofluids, the pressure drop is 3.3%; for MWCNTS nanofluids, the pressure drop is 4.4%; and for Ag with MWCNTS nanofluids in a 1:1 ratio, the pressure drop is 10.4%. These values are relative to the pressure drop in a bare channel.

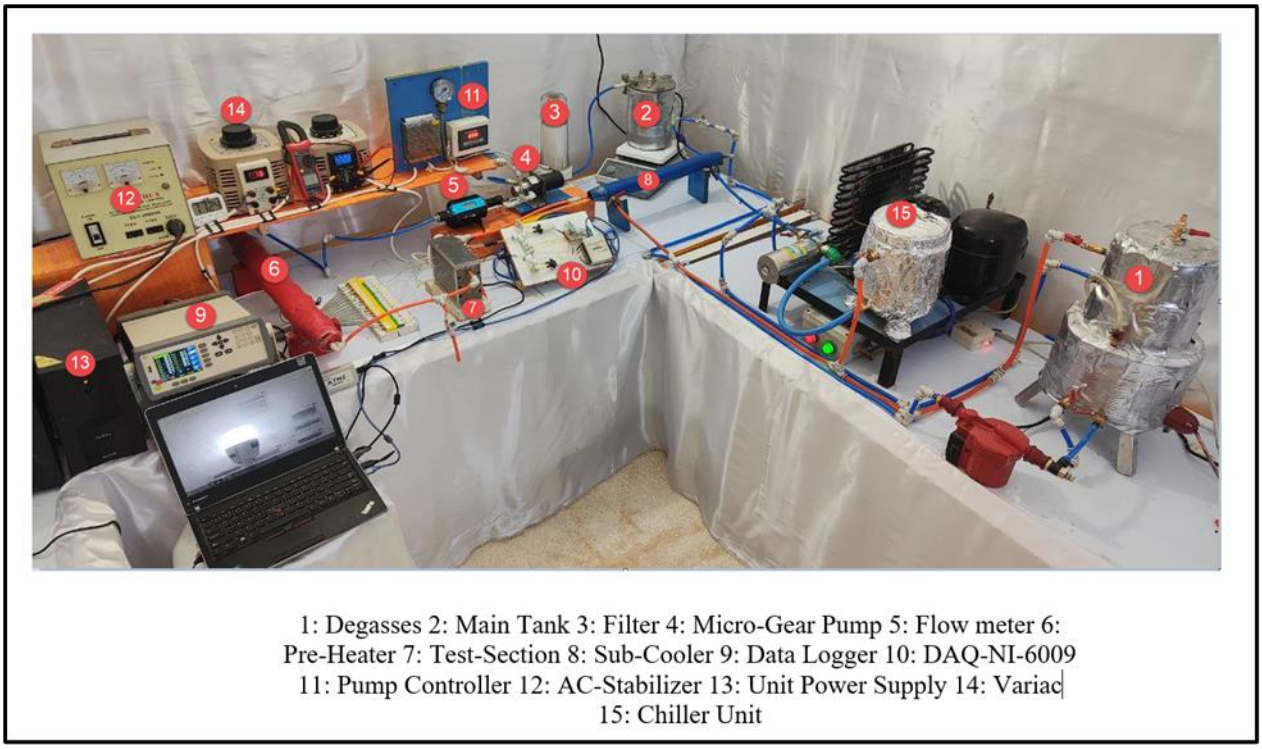

Plate 1. Experimental facility

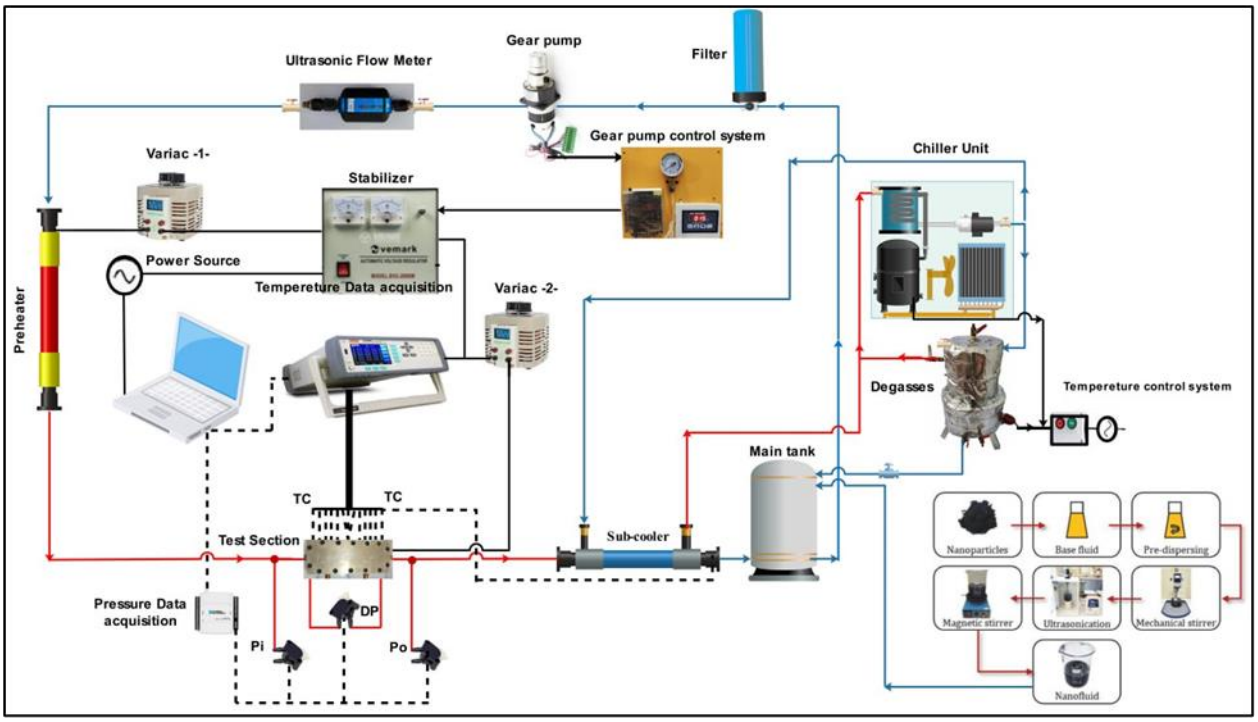

Figure 1. Detailed schematic of the laboratory

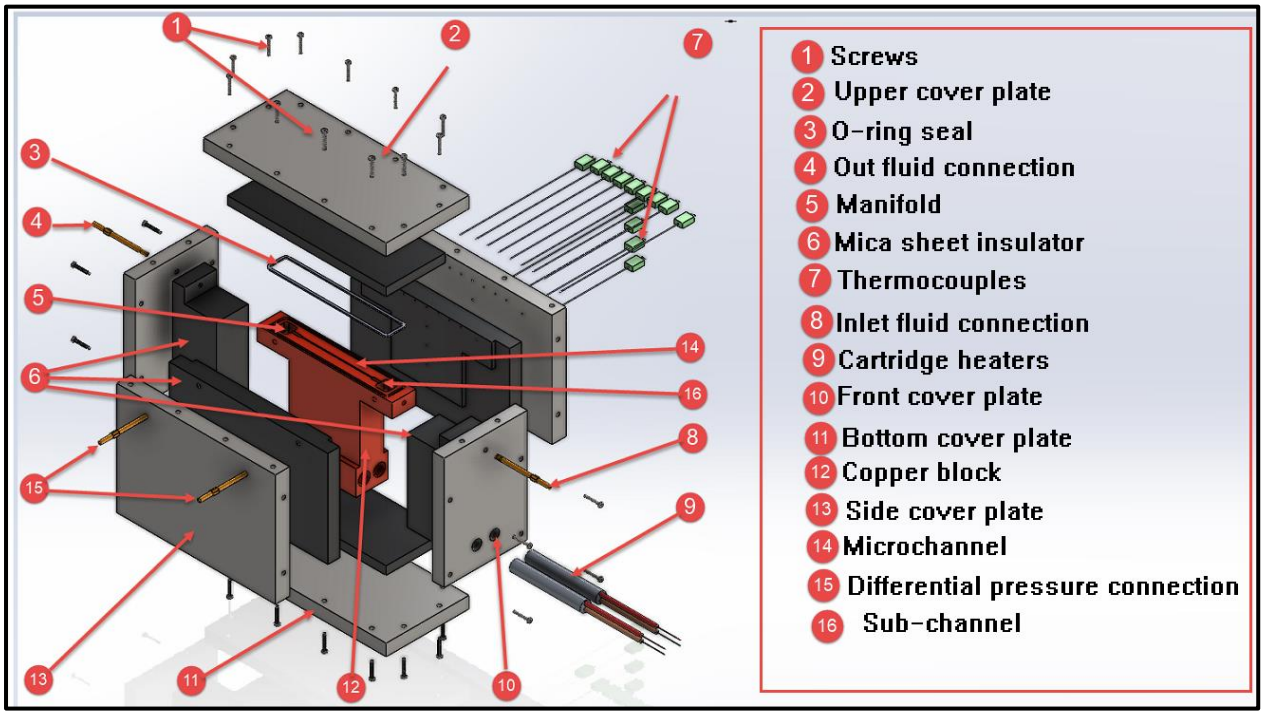

Figure 2. Test section diagram

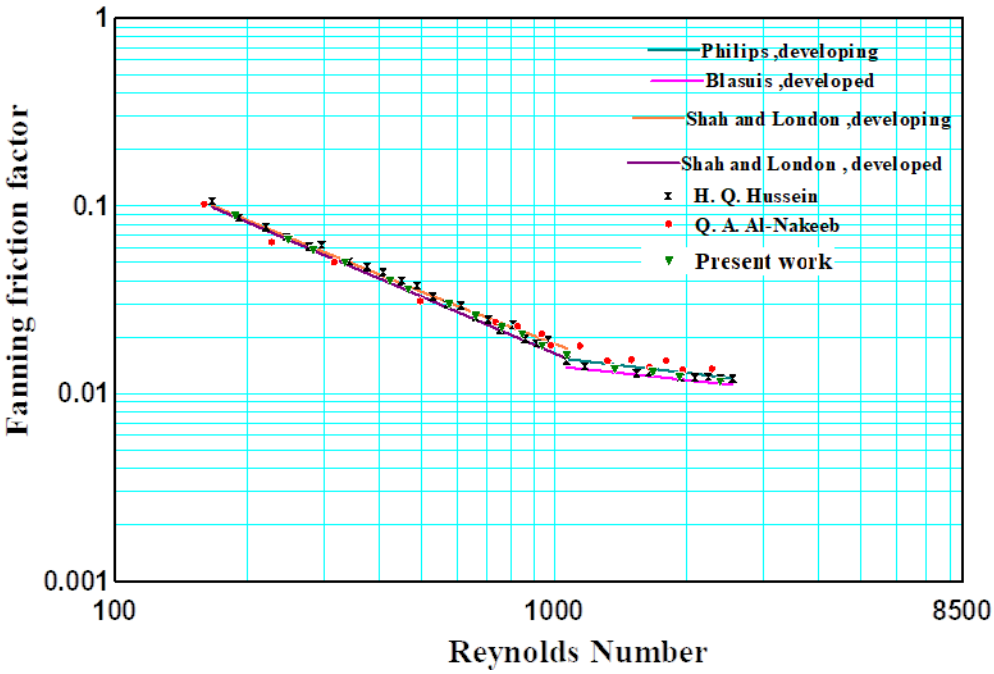

Figure 3 Experimental results of Fanning friction factor compared with the correlations of laminar and turbulent flow for microchannel.

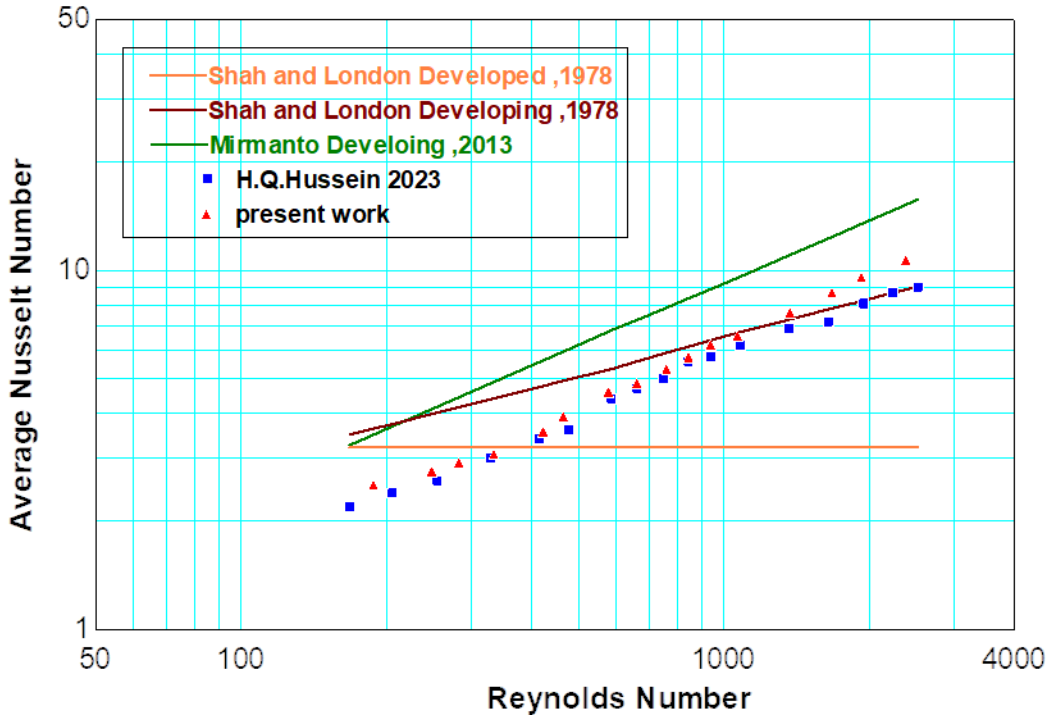

Figure 4 Comparison of experimental microchannel results with the correlations of laminar flow and experimental average Nusselt numbers.

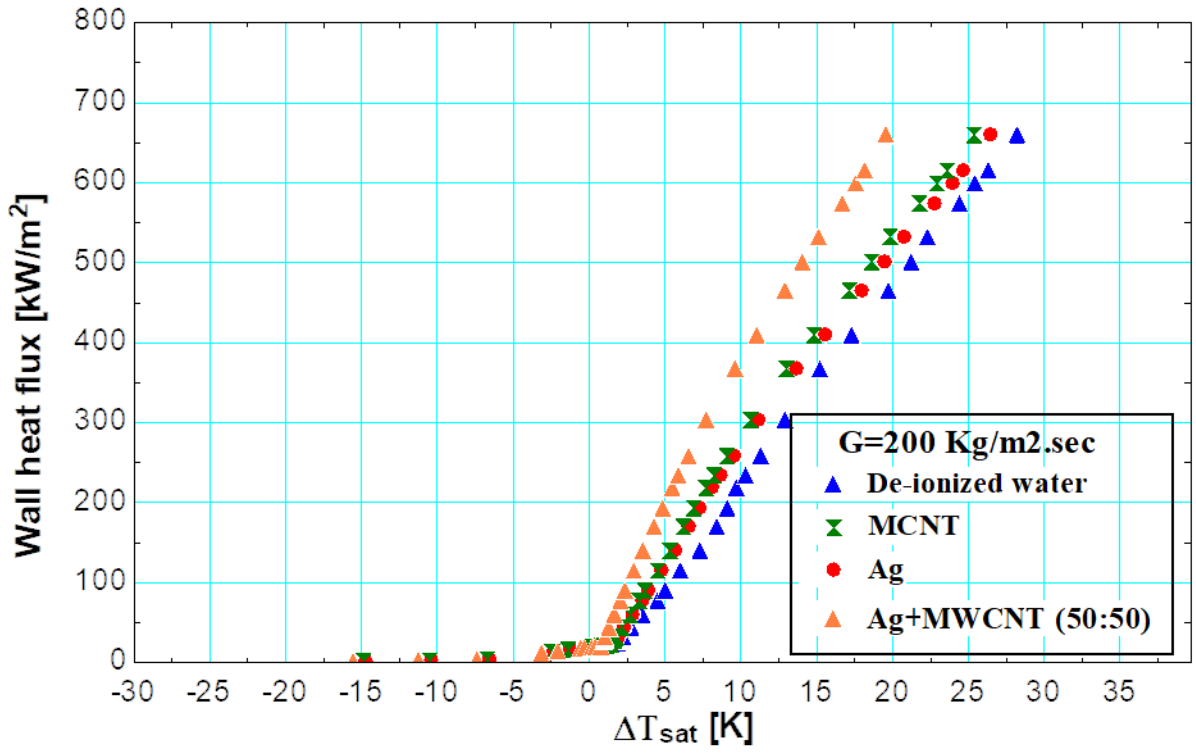

Figure 5 Boiling curve microchannel over different models at sub-cooled 20K

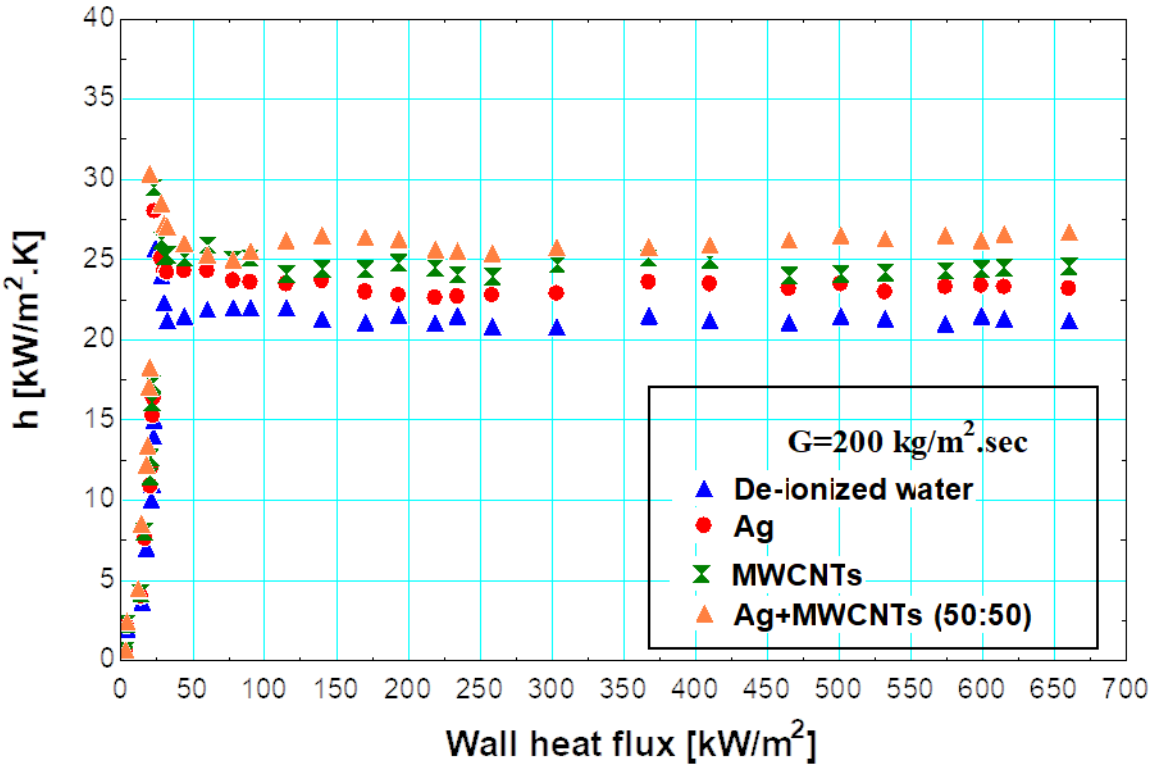

Figure 6 Coefficient of local heat transfer versus exit vapor quality over various models for a degree of subcooling of 20K at a location of Z/Lch=0.98

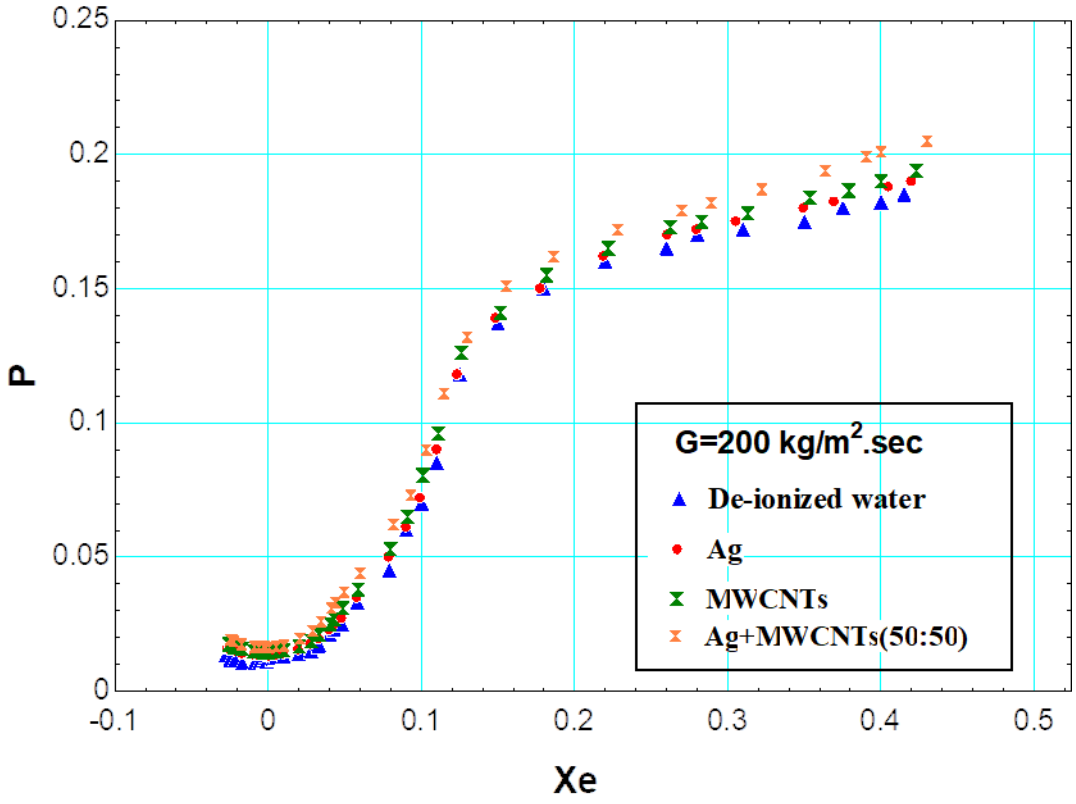

Figure 7 The drop in pressure versus the exit vapor quality over different models at sub-cooled 20 K.

References

[1] S. G. Kandlikar and W. J. Grande, "Evolution of microchannel flow passages-thermohydraulic performance and fabrication technology," Heat Transf. Eng., vol. 24, no. 1, pp. 3–17, Jan. 2003, doi: 10.1080/01457630304040.

[2] T. Harirchian and S. V. Garimella, "Microchannel size effects on local flow boiling heat transfer to a dielectric fluid," International Journal of Heat and Mass Transfer, vol. 51, no. 15–16. pp. 3724–3735, 2008, doi: 10.1016/j.ijheatmasstransfer.2008.03.013.

[3] H. Huang, N. Borhani, and J. R. Thome, "Experimental investigation on flow boiling pressure drop and heat transfer of R1233zd(E) in a multi-microchannel evaporator," Int. J. Heat Mass Transf., vol. 98, pp. 596–610, Jul. 2016, doi: 10.1016/j.ijheatmasstransfer.2016.03.051.

[4] B. Markal, O. Aydin, and M. Avci, "An experimental investigation of saturated flow boiling heat transfer and pressure drop in square microchannels," International Journal of Refrigeration, vol. 65. pp. 1–11, 2016, doi: 10.1016/j.ijrefrig.2015.12.013.

[5] S. A. Mohammed and E. M. Fayyadh, "Experimental Investigation of Heat Transfer and Flow Characteristics in Different Inlet Subcooled Flow Boiling in Microchannel," IOP Conf. Ser. Mater. Sci. Eng., vol. 671, no. 1, p. 012023, Jan. 2020, doi: 10.1088/1757-899X/671/1/012023.

[6] Q. A. Al-Nakeeb, E. M. Fayyadh, and M. R. Hasan, "Experimental Investigation on Sub-Cooled Degree Effect on the Flow Boiling in a Microchannel Heat Sink," 2023, pp. 303–330.

[7] A. H. Al-Zaidi, M. M. Mahmoud, and T. G. Karayiannis, "Flow boiling of HFE-7100 in microchannels: Experimental study and comparison with correlations," Int. J. Heat Mass Transf., vol. 140, pp. 100–128, 2019, doi: 10.1016/j.ijheatmasstransfer.2019.05.095.

[8] T. Harirchian and S. V. Garimella, "Microchannel size effects on local flow boiling heat transfer to a dielectric fluid," International Journal of Heat and Mass Transfer, vol. 51, no. 15–16. pp. 3724–3735, 2008, doi: 10.1016/j.ijheatmasstransfer.2008.03.013.

[9] S. S. Bertsch, E. A. Groll, and S. V. Garimella, "Effects of heat flux, mass flux, vapor quality, and saturation temperature on flow boiling heat transfer in microchannels," International Journal of Multiphase Flow, vol. 35, no. 2. pp. 142–154, 2009, doi: 10.1016/j.ijmultiphaseflow.2008.10.004.

[10] E. M. Fayyadh, M. M. Mahmoud, K. Sefiane, and T. G. Karayiannis, "Flow boiling heat transfer of R134a in multi microchannels," Int. J. Heat Mass Transf., vol. 110, pp. 422–436, Jul. 2017, doi: 10.1016/j.ijheatmasstransfer.2017.03.057.

[11] E. Costa-Patry, J. Olivier, B. A. Nichita, B. Michel, and J. R. Thome, "Two-phase flow of refrigerants in 85μm-wide multi-microchannels: Part I - Pressure drop," Int. J. Heat Fluid Flow, vol. 32, no. 2, pp. 451–463, 2011, doi: 10.1016/j.ijheatfluidflow.2011.01.005.

[12] B. Agostini, J. R. Thome, M. Fabbri, B. Michel, D. Calmi, and U. Kloter, "High heat flux flow boiling in silicon multi-microchannels - Part I: Heat transfer characteristics of refrigerant R236fa," International Journal of Heat and Mass Transfer, vol. 51, no. 21–22. pp. 5400–5414, 2008, doi: 10.1016/j.ijheatmasstransfer.2008.03.006.

[13] T. Alam et al., "Force analysis and bubble dynamics during flow boiling in silicon nanowire microchannels," Int. J. Heat Mass Transf., vol. 101, pp. 915–926, 2016, doi: 10.1016/j.ijheatmasstransfer.2016.05.045.

[14]Shah, R.K., London, A.L. (1978). Laminar Flow Forced Convection in Ducts. Elsevier.

.[15]Blasius, H. Ähnlichkeitsgesetz bei Reibungsvorgängen in Flüssigkeiten, Forschg. Arb. Ing.-Wes., 131, 1913.

[16] Phillips R.J. (1987), Forced-Convection, Liquid-Cooled, MicrochannelHeat Sinks, MSc thesis, Massachusetts Institute of Technolog, Cambridge,USA

[17]Al-Nakeeb, Q.A., Fayyadh, E.M., Hasan, M.R. (2022). Experimental investigation of artificial cavities effect of single-phase fluid flow and heat transfer in single microchannel. Engineering and Technology Journal, 40(1): 109-119. http://doi.org/10.30684/etj.v40i1.2122

[18]Hussein, Hasan Q., Ekhlas M. Fayyadh, and Moayed R. Hasan. "Investigating the effect of electroplated coatings on single-phase fluid flow and heat transfer in microchannel." Engineering and Technology Journal 42.1 (2024): 117-134.

[19] Mirmanto M. (2016), “Local pressure measurements and heat transfercoefficients of flow boiling in a rectangular microchannel”, Heat and MassTransfer, Springer Berlin Heidelberg, Vol. 52 No. 1, pp. 73–83.

[20] Benkheira L., Souhar M., and Baudouy B. (2006), “Heat and mass transfer in nucleate boiling regime of HE I in a natural circulation loop”, AIPConference Proceedings, Vol. 823 I, pp. 871–878.

[21] Balasubramanian K., Jagirdar M., Lee P.S., Teo C.J., and Chou S.K.(2013), “Experimental investigation of flow boiling heat transfer andinstabilities in straight microchannels”, Heat and Mass Transfer, ElsevierLtd, Vol. 66, pp. 655–671.

[22] Qu W., and Mudawar I. (2003), “Flow boiling heat transfer in two-phase micro-channel heat sinks-I. Experimental investigation and assessment of correlation methods”, International Journal of Heat and Mass Transfer, Vol. 46 No. 15, pp. 2755–2771.

[23] T. Harirchian and S. V. Garimella, “Microchannel size effects on local flow boiling heat transfer to a dielectric fluid,” International Journal of Heat and Mass Transfer, vol. 51, no. 15–16. pp. 3724–3735, 2008, doi: 10.1016/j.ijheatmasstransfer.2008.03.013.

[24] S. A. Mohammed and E. M. Fayyadh, “Experimental Study on Heat Transfer and Flow Characteristics in Subcooled Flow Boiling in a Microchannel,” Journal of Engineering, vol. 26, no. 9. pp. 173–190, 2020, doi: 10.31026/j.eng.2020.09.12.